JOURNAL OF COMPUTATIONAL PHYSICS 110, 292-300 (1994)

Effects of Mass Discontinuity on the Numerical Solutions to Quantum Wells Using the Effective Mass Equation

TSUNG L. LI AND KELIN J. KUHN

Department of Electrical Engineering, FT-10, University of Wahington, Seattle, Washington 98195

Received August 21, 1991; revised November 30, 1992

This paper investigates the effects of mass dicontinuity on the numerical solutions to quantum wells using the effective mass equation. The numerical methods utilized are the finite element method with first-order elements, and the finite difference method with the entire truncated solution domain discretized by equally spaced nodes. The three Hamiltonians explored are the convention Hamiltonian, the BenDaniel and Duke Hamiltonian, and the Bastard Hamiltonian. It is shown that the proper discretization patterns for both numerical schemes may drastically improve the solution accuracy. The finite difference representation of the BenDaniel and Duke Hamiltonian using the direct mass average is found more accurate than the one using the harmonic mass average. It is further pointed out that, at the mass profile discontinuities, the commonly accepted interface conditions for the Bastard Hamiltonian are not natural conditions. This observation is critical if the Bastard Hamiltonian is to be solved numerically.

1. INTRODUCTION

The single-band effective mass approach is widely used in quantum well problems [1–5]. The envelope function ψ satisfies the effective mass equation,

$$\hat{H}\psi = E\psi, \tag{1}$$

where $\hat{H}$ is the Hamiltonian operator and E is the eigenenergy. Since the effective mass and the potential energy depend on the location, the Hamiltonian is position-dependent. The eigensolutions to the effective mass equation (1) are indispensable to the investigation of the properties of quantum wells.

There are several analytical means in the literature to solve the effective mass equation (1) for heterostructures such as quantum wells and superlattices. The most commonly used method is to solve the transcendental equation obtained by matching the appropriate interface conditions for the envelope functions. The two interface conditions usually used are the continuity of (1) the envelope functions and (2) the first derivatives of the envelope functions, or the first derivatives of the envelope functions divided by the mass. For a heterojunction not subject to an external field, propagating and evanescent plane waves are used for the envelope functions [2, 6, 7]. Airy functions are used for the envelope functions in the presence of a uniform static electric field [8–13]. Usually, the exact solutions to piecewise linear structures are obtainable by this transfer matrix type of methodology.

The approximate solutions to Eq. (1) are explored by several researchers, using Fourier transformation [14], Green's functions [15], the perturbation method [16], and the variational method [17]. The variational method is based on the fact that the envelope function that satisfies Eq. (1) is the one that makes the following functional stationary [18]

$$\langle E \rangle_\psi = \frac{\langle \psi | \hat{H} | \psi \rangle}{\langle \psi | \psi \rangle}. \tag{2}$$

The effective mass equation (1) has also been solved by two numerical methods. The first method is the finite difference method with equally spaced discretizations [4, 5]. The second one is the finite element method. The finite element method has been applied to problems in nuclear physics [19], and in atomic and molecular physics [20–22] after the first introduction by Askar to quantum mechanics [23]. Recently the optimal finite-element mesh that minimizes the energy excess has been reported and the results for an infinite quantum well have been generated [24]. K. Nakamura *et al.* first applied the finite element method to incorporate the Ando's interface conditions at the heterojunctions [25–27]. But, the effects of the effective mass profile discontinuity on either numerical method have not yet been studied.

The finite element method [28, 29] and the variational method share the same fundamental concept as stated in Eq. (2). The difference is that the variational method approaches stationarity by presuming a formal envelope

0021-9991/94 $6.00

function with inserted parameters which are undetermined. Then $\langle E\rangle_\psi$ is minimized with respect to these parameters [17]. The number of undetermined parameters cannot be many so as to elude the complexity of the $\langle E\rangle_\psi$ expression. The accuracy of the solution greatly relies on the proposition of the formal envelope function. On the other hand, the finite element method has the simplicity of using low-order polynomials as basis functions to approximate the real envelope function and the flexibility of increasing the number of nodal points without complicating the formulation.

Although there are means to obtain the exact solutions to quantum wells with piecewise linear profiles, numerical methods become important if the quantum well profiles are not linear or if the physical phenomena induced by the many-body effects such as Coulomb and exchange interactions are considered [8, 30, 31].

In this paper, a comparison of the finite element and the finite difference solutions to a finite square quantum well and a simple harmonic oscillator will be presented to illustrate the effects of the mass discontinuity. With the discontinuous mass, the discretization patterns become important to the solution accuracy. The BenDaniel and Duke Hamiltonian has two finite difference equations: one uses the direct average for the mass; the other uses the harmonic average. It will be shown that the direct average is preferable to the harmonic average. It will be shown that the direct average is preferable to the harmonic average.

It was claimed in Ref. [5] that the Bastard Hamiltonian is inappropriate to treat heterojunctions because it produces discontinuous envelope functions. This paper will show that the inappropriateness results from the lack of essential interface conditions at the heterojunction and that it is fallacious to solve the Bastard Hamiltonian by the finite difference method without additional conditions at the interface.

2. GOVERNING EQUATIONS AND NUMERICAL METHODS

Due to the location-dependence of the effective mass, there is no unique form for the Hamiltonian in Eq. (1) [32–35]. Three frequently used Hamiltonians will be investigated in this paper: the conventional Hamiltonian, the BenDaniel and Duke Hamiltonian, and the Bastard Hamiltonian. In this section, the governing equations derived from the three Hamiltonians will be given in the first subsection; the finite element and finite difference formulations will be presented in the next two subsections.

2.1. *Governing Equations*

The effective mass equation employing the conventional Hamiltonian, the BenDaniel and Duke Hamiltonian, and the Bastard Hamiltonian takes the following forms:

Conventional Hamiltonian,

$$-\frac{\hbar^2}{2m(z)}\frac{d^2\psi(z)}{dz^2}+V(z)\,\psi(z)=E\psi(z), \tag{3}$$

BenDaniel and Duke Hamiltonian,

$$-\frac{\hbar^2}{2}\frac{d}{dz}\left[\frac{1}{m(z)}\frac{d\psi(z)}{dz}\right]+V(z)\,\psi(z)=E\psi(z), \tag{4}$$

Bastard Hamiltonian,

$$-\frac{\hbar^2}{4}\left[\frac{1}{m(z)}\frac{d^2\psi(z)}{dz^2}+\frac{d^2}{dz^2}\frac{\psi(z)}{m(z)}\right]+V(z)\,\psi(z)=E\psi(z), \tag{5}$$

where z, $m(z)$, and $V(z)$ are the location, the effective mass, and the confinement potential, respectively.

For the bounded levels of the electron, the boundary conditions read

$$\psi(z=\pm\infty)=0. \tag{6}$$

The boundary conditions encompass an infinite domain, and this is not achievable for the numerical schemes employing a finite number of finite-sized meshes. Usually, these conditions are replaced by the approximate boundary conditions [36],

$$\psi(x_1)=\psi(x_2)=0, \tag{7}$$

where x_1 and x_2 are positions at which the envelope functions are sufficiently insignificant.

Inspecting both sides of Eqs. (3) and (4), it follows that both the conventional Hamiltonian and the BenDaniel and Duke Hamiltonian satisfy the continuity of the envelope function at the discontinuous point of the mass z_0,

$$\psi(z_0^-)=\psi(z_0^+). \tag{8}$$

Integrating both sides of Eqs. (3) and (4) across z_0, the conventional Hamiltonian gives

$$\frac{d\psi(z_0^-)}{dz}=\frac{d\psi(z_0^+)}{dz}, \tag{9}$$

but the BenDaniel and Duke Hamiltonian yields,

$$\frac{1}{m(z_0^-)}\frac{d\psi(z_0^-)}{dz}=\frac{1}{m(z_0^+)}\frac{d\psi(z_0^+)}{dz}. \tag{10}$$

Equation (10) is usually interpreted as the continuity of the probability flux [37]. Since Eqs. (8) to (10) follow directly from the governing equations (3) and (4), they are regarded as *natural* interface conditions.

The interface conditions given in Eqs. (8) and (10) were claimed derivable by integrating the Bastard Hamiltonian in Eq. (5) across the interface in Ref. [1]; namely, they were treated as natural conditions for the Bastard Hamiltonian. However, this assertion is *not* true and can mislead researchers who try to solve the Bastard Hamiltonian by numerical methods [5]. In the following paragraphs, it will be shown that the envelope functions are unbounded at the abrupt heterojunction unless some interface conditions are imposed essentially.

Suppose that the envelope function solution to Eq. (5) is continuous at an interface point $z = z_0$, then $d^2[\psi(z)/m(z)]/dz^2$ is singular to the order of $d/dz[\delta(z-z_0)]$, but $1/m(z)\cdot d^2\psi(z)/dz^2$ is at most singular to the order of $\delta(z-z_0)$ because $m(z)$ has an abrupt jump at z_0. Therefore, the envelope function fails to be continuous at all interface points.

Furthermore, Eq. (5) can be written as

$$-\frac{\hbar^2}{2}\frac{d}{dz}\left[\frac{1}{m(z)}\frac{d\psi(z)}{dz}\right] + \left[-\frac{\hbar^2}{2}\frac{1}{m(z)^3}\left(m'(z)^2-\frac{1}{2}m(z)\,m''(z)\right)+V(z)\right]\times\psi(z)=E\psi(z), \tag{11}$$

where $m'(z)=dm(z)/dz$ and $m''=d^2m(z)/dz^2$. Assume that $\psi(z)$ is bounded in the vicinity of an interface point, z_0, integrating both sides of Eq. (11) across the interface point gives

$$\left[\frac{1}{m(z)}\frac{d\psi(z)}{dz}\right]\Bigg|_{z_0^-}^{z_0^+} = -\int_{z_0^-}^{z_0^+}\left[\frac{1}{m(z)^3}\left(m'(z)^2-\frac{1}{2}m(z)\,m''(z)\right)\right]\psi(z)\,dz. \tag{12}$$

The right-hand side of Eq. (12) is not convergent because it involves the integration of $[\delta(z-z_0)]^2$. In other words,

$$\left[\frac{1}{m(z)}\frac{d\psi(z)}{dz}\right]\Bigg|_{z_0^-}^{z_0^+} \quad \text{diverges,} \tag{13}$$

which implies that both $d\psi(z_0^-)/dz$ and $d\psi(z_0^+)/dz$ diverge. Hence, $|\psi(z)|$ tends to infinity as z approaches z_0; that is, $\psi(z)$ is not bounded.

Conclusively, when the Bastard Hamiltonian is applied to a structure with abrupt effective mass change, the envelope function does not possess the continuity properties stated in Eqs. (9), (8), and (10). Thus, the interface conditions given in Eqs. (8) and (10) are *not* natural conditions.

The solutions to the conventional Hamiltonian (3), the BenDaniel and Duke Hamiltonian (4), and the Bastard Hamiltonian (5) are identical within the interval with a constant mass and a constant potential because all Hamiltonians reduce to the same differential form. If the interface conditions given by Eqs. (8) and (10) are essentially imposed on the Bastard Hamiltonian, the solutions to the Bastard Hamiltonian are same as the BenDaniel and Duke Hamiltonian [9].

2.2. *The Finite Element Method*

Each of the three Hamiltonians in Eqs. (3) to (5) is a special case of a general second-order self-adjoint eigenproblem,

$$-\frac{d}{dz}\left[\alpha(z)\frac{d\psi(z)}{dz}\right]+\beta(z)\,\psi(z)-E\gamma(z)\,\psi(z)=0. \tag{14}$$

For the conventional Hamiltonian,

$$\alpha(z)=\frac{\hbar^2}{2}, \qquad \beta(z)=m(z)\,V(z), \qquad \gamma(z)=m(z).$$

For the BenDaniel and Duke Hamiltonian,

$$\alpha(z)=\frac{\hbar^2}{2}\frac{1}{m(z)}, \qquad \beta(z)=V(z), \qquad \gamma(z)=1.$$

For the Bastard Hamiltonian, $\alpha(z)$ and $\gamma(z)$ are same as the BenDaniel and Duke Hamiltonian, and

$$\beta(z)=\frac{\hbar^2}{2}\frac{1}{m(z)^3}\left[m'(z)^2-\frac{1}{2}m(z)\,m''(z)\right]+V(z). \tag{15}$$

From the finite element formulation, the differential eigenproblem becomes a linear eigenproblem,

$$\mathbf{K}\cdot\mathbf{\Psi}=E\cdot\mathbf{M}\cdot\mathbf{\Psi}. \tag{16}$$

$\mathbf{K}$ and $\mathbf{M}$ are the stiffness and the mass matrices, respectively, and are given as

$$\mathbf{K}=\int_{x_1}^{x_2}[\mathbf{N}'^{\mathrm{T}}\alpha(z)\,\mathbf{N}'+\mathbf{N}^{\mathrm{T}}\beta(z)\,\mathbf{N}]\,dz \tag{17}$$

and

$$\mathbf{M}=\int_{x_1}^{x_2}\mathbf{N}^{\mathrm{T}}\gamma(z)\,\mathbf{N}\,dz, \tag{18}$$

where $\mathbf{\Psi}=[\psi_1,\psi_2,...,\psi_M]$, $\mathbf{N}=[N_1,N_2,...,N_M]$, and $\mathbf{N}'=d\mathbf{N}/dz$. N_i and ψ_i are the basis function and the nodal value at the ith node, respectively, for $i=1,2,...,M$. M is the number of nodes.

In this paper, linear shape functions are utilized; thus both **K** and **M** are tridiagonal and symmetric. **K** and **M** can be assembled from element matrices given by

$$\mathbf{K}^{(e)} = \int_0^1 \begin{bmatrix} \alpha(\eta)/h_e + h_e(1-\eta)^2\beta(\eta) & -\alpha(\eta)/h_e + h_e\eta(1-\eta)\beta(\eta) \\ -\alpha(\eta)/h_e + h_e\eta(1-\eta)\beta(\eta) & \alpha(\eta)/h_e + h_e\eta^2\beta(\eta) \end{bmatrix} d\eta, \tag{19}$$

and

$$\mathbf{M}^{(e)} = h_e \int_0^1 \begin{bmatrix} (1-\eta)^2\gamma(\eta) & \eta(1-\eta)\gamma(\eta) \\ \eta(1-\eta)\gamma(\eta) & \eta^2\gamma(\eta) \end{bmatrix} d\eta, \tag{20}$$

where h_e is length of the element and η is the local coordinate. η is related to the global coordinate by $z = h_e\eta + x_e$, where x_e is the global coordinate of the left end of the element. In this paper, the integrations in the element matrices, $\mathbf{K}^{(e)}$ and $\mathbf{M}^{(e)}$ are calculated by eight-point Gaussian quadrature [38].

From Eqs. (15) and (19), the effective mass must be at least be a C^1 function for the finite element formulation of the Bastard Hamiltonian to be valid. (C^1 denotes the set of functions whose first derivatives are continuous.)

2.3. *The Finite Difference Method*

The finite difference method is gaining its popularity on solving the effective mass equations given in Eqs. (3) to (5). The entired truncated solution domain is discretized by equally spaced nodal points. The difference equations are given below.

The solution domain $[x_1, x_2]$ is discretized to N meshes of equal size. The mesh length becomes $\Delta z = (x_2 - x_1)/N$. Then the central difference method is used. Some notational conventions employed throughout this subsection are $m_i = m(z_i)$, $V_i = V(z_i)$, and $\psi_i = \psi(z_i)$, where $z_i = x_1 + i \cdot \Delta z$ is the coordinate of the ith nodal point, for $i = 0, 1, 2, ..., N$. The vanishing boundary conditions at $z = x_1$ and $z = x_2$ given in Eq. (7) are translated to $\psi_0 = \psi_N = 0$.

The finite difference equation of the conventional Hamiltonian (3) can be written as

$$-\frac{\hbar^2}{2(\Delta z)^2}\frac{1}{m_i}\psi_{i-1} + \left[\frac{\hbar^2}{(\Delta z)^2}\frac{1}{m_i} + V_i\right]\psi_i - \frac{\hbar^2}{2(\Delta z)^2}\frac{1}{m_i}\psi_{i+1} = E\psi_i, \tag{21}$$

for $i = 1, 2, ..., N-1$. When expressed in matrix form, it is tridiagonal, but asymmetric.

Mathematically, the differential term, $d/dz[1/m(z) \cdot d\psi(z)/dz]$, of the BenDaniel and Duke Hamiltonian (4) is undefined at the mass discontinuities. The indefiniteness of the function values introduces the ambiguity of the numerical schemes. In general, the value at the middle of the ith mesh $((1/m(z))|_{i+1/2})$ can be approximated by $m_{i+1/2}$ given by

$$(m_{i+1/2})^\theta = \tfrac{1}{2}[(m_i)^\theta + (m_{i+1})^\theta], \tag{22}$$

where θ is a real number. If $\theta = 1$, Eq. (22) results in the direct average of the nodal values of the mass. If $\theta = -1$, Eq. (22) becomes the harmonic average. The finite difference equations for the BenDaniel and Duke Hamiltonian obtained by the θ values of 1 and -1 are termed the direct difference equation (23) and the harmonic difference equation (24), respectively,

$$-\frac{\hbar^2}{(\Delta z)^2}\left(\frac{1}{m_{i-1}+m_i}\right)\psi_{i-1} + \left[\frac{\hbar^2}{(\Delta z)^2}\left(\frac{1}{m_{i-1}+m_i} + \frac{1}{m_i+m_{i+1}}\right) + V_i\right]\psi_i - \frac{\hbar^2}{(\Delta z)^2}\left(\frac{1}{m_i+m_{i+1}}\right)\psi_{i+1} = E\psi_i \tag{23}$$

and

$$-\frac{\hbar^2}{4(\Delta z)^2}\left(\frac{1}{m_{i-1}} + \frac{1}{m_i}\right)\psi_{i-1} + \left[\frac{\hbar^2}{4(\Delta z)^2}\left(\frac{1}{m_{i-1}} + \frac{2}{m_i} + \frac{1}{m_{i+1}}\right) + V_i\right]\psi_i - \frac{\hbar^2}{4(\Delta z)^2}\left(\frac{1}{m_i} + \frac{1}{m_{i+1}}\right)\psi_{i+1} = E\psi_i, \tag{24}$$

for $i = 1, 2, ..., N-1$. Both the direct and the harmonic difference equations are tridiagonal and symmetric.

The difference equation for the Bastard Hamiltonian (5) is

$$-\frac{\hbar^2}{(2\Delta z)^2}\left(\frac{1}{m_i} + \frac{1}{m_{i-1}}\right)\psi_{i-1} + \left[\frac{\hbar^2}{(\Delta z)^2}\left(\frac{1}{m_i}\right) + V_i\right]\psi_i - \frac{\hbar^2}{(2\Delta z)^2}\left(\frac{1}{m_i} + \frac{1}{m_{i+1}}\right)\psi_{i+1} = E\psi_i, \tag{25}$$

for $i = 1, 2, ..., N-1$. This is also tridiagonal and symmetric.

It will be shown in the next section that the discretization pattern for the finite difference plays an important role in the numerical solution to the quantum well with a discontinuous mass profile. A proper discretization pattern generates more accurate solutions than an improper pattern. The terminology of proper and improper patterns is first defined here. The proper discretization pattern for the finite difference is the pattern which satisfies two requirements: (1) the mass discontinuity coincides with a

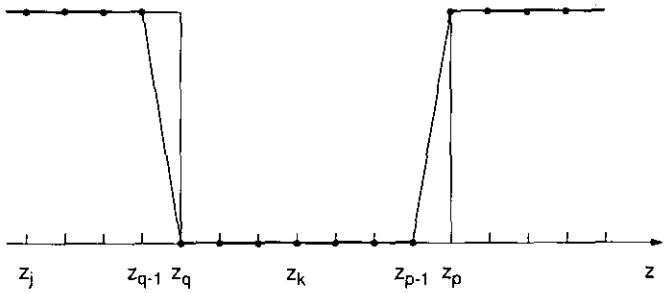

FIG. 1. *An example of the proper discretization pattern of a SQW.* Only one end point of the well is regarded as belonging to its interior. The other end point is considered exterior to the well. Consequently, the average well width remains same as a sharp SQW.

nodal point, and (2) exactly one of the two adjacent mass discontinuities can be treated interior to the mass profile segment defined by these two discontinuous points. The second requirement is to preserve the average well width of the discretized representation of a quantum well. An example of a proper discretization pattern for a square quantum well is depicted in Fig. 1.

3. NUMERICAL RESULTS AND DISCUSSIONS

In this section, the finite element and the finite difference solution to a square quantum well (SQW) and a simple harmonic oscillator (SHO) are presented. A simple harmonic oscillator is characterized by a quadratic barrier and a constant particle mass. There are two reasons to choose working on a SQW and a SHO. First, the mass profile of a SQW exhibits finite discontinuities, but that of a SHO is continuous. Comparison of the solutions to a SQW and a SHO obtained by the same Hamiltonian and numerical scheme reveals the effect of discontinuity on the solution. Second, both the SQW and the SHO are analytically solvable. The transfer matrix method is applied to the SQW for the analytic solution [39]. The analytic solution to a SHO is well established [37]. Numerical eigenvalues are compared with analytic solutions to demonstrate the effects of the mass discontinuity on various computational schemes.

These calculations will be performed on the conduction band of a structure fabricated by *GaAs* and $Al_xGa_{1-x}As$, where x is the composition fraction of *Al*. The band-gap energy and the effective mass for $Al_xGa_{1-x}As$ take the following relations [40], for $0 \leqslant x \leqslant 0.45$,

$$E_g(Al_xGa_{1-x}As) = \delta + vx \qquad \text{(eV)}, \tag{26}$$

and

$$m(Al_xGa_{1-x}As) = \alpha + \mu x, \tag{27}$$

where $\delta = 1.424$, $v = 1.247$, $\alpha = 0.067m_0$, and $\mu = 0.083m_0$. (m_0 is the electron rest mass.) Moreover, the band-offset ratio of 0.80:0.20 is taken for all subsequent calculations.

Both the finite element and the finite difference methods eventually lead to a linear algebraic eigenproblem. The subroutine, SSPACE, in Ref. [41] is used to solve the eigenproblem, where the convergence tolerance on eigenvalues is taken as 10^{-15}. The calculations are implemented in C language and computed on an IBM3090-300E machine running AIX 370.

The numerical results of SQW and SHO structures are discussed in the following two subsections.

3.1. *Square Quantum Well*

The well width of the SQW is $L = 96.11$ Å (34 monolayers), and its barrier height is $V_0 = 0.400$ eV. The effective masses in the barrier and the well are $0.100m_0$ and $0.067m_0$, respectively. This SQW is equivalent to the conduction band of a $GaAs$-$Al_{0.401}Ga_{0.599}As$ structure.

For each Hamiltonian, four numerical schemes are used to solve the SQW and their accuracy is investigated. These four schemes are the finite element method (FEM) with proper and improper discretization patterns and the finite difference (FD) method with proper and improper discretization patterns. The relative error is defined as the ratio of the error of the numerical eigenvalue to the analytic solution ($|E_i - E_i^{\text{analytic}}|/E_i^{\text{analytic}}$, for the ith level). The end points of the numerical solution domain used to produce results in this subsection are $x_1 = -x_2 = 3.5L$.

Conventional Hamiltonian. The relative errors of the numerical methods versus the number of discretizations N are shown in Fig. 2. The results by a proper discretization

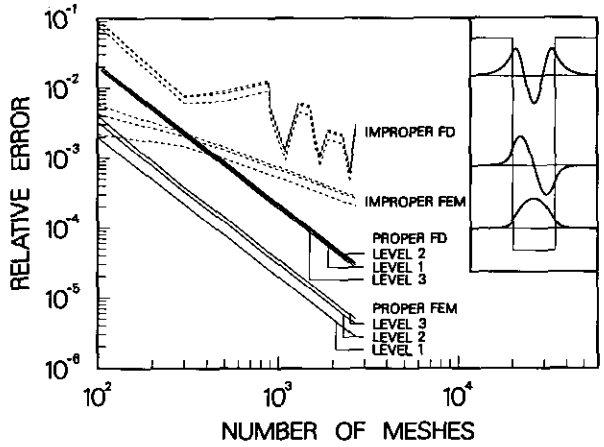

FIG. 2. *Accuracy of SQW solution using the conventional Hamiltonian.* The relative error ($|E_i - E_i^{\text{analytic}}|/E_i^{\text{analytic}}$) versus the discretization number (N) for the FEM and FD solutions with proper and improper discretization patterns is plotted. The solutions by the proper discretization patterns are in solid lines; those by the improper discretization patterns are in dashed lines. The location of the discontinuous point is randomly placed in the mesh for the improper FD solutions. However, the location of the discontinuous point is kept at a fixed fractional distance in the mesh for the improper FEM solutions. The envelope functions shown in the window confirm the natural interface conditions.

pattern are depicted by solid lines; those by an improper discretization pattern are by dashed lines. The properly discretized patterns introduce less numerical errors than the improperly discretized patterns for both the FEM and the FD schemes. It is found that, for both methods, the relative errors of the improper discretization pattern depend on the location of the discontinuous point in the mesh. If the discontinuous points are randomly placed in the mesh, the relative error as a function of N oscillates as illustrated by the zigzag dashed line for the FD results in Fig. 2. If the discontinuous points are located at a fixed fractional place of the mesh, say, three quarters from the left end of the mesh, the relative error steadily decreases as shown by the dashed line for the FEM results in Fig. 2. Note that the relative errors of the FD with an improper discretization pattern are rarely below 10^{-3}. With the solution domain properly discretized, the FEM and the FD solutions reveal monotonic convergence as the discretization number increases.

In the FEM solution, rather than equally spaced, the nodal points are distributed more densely over the place where the magnitude of the envelope function is larger. Owing to this nonuniform distribution of meshes, the FEM solutions are about 10 times more accurate than the equally spaced FD solutions.

The envelope functions are plotted in the window of Fig. 2. The envelope functions and their derivatives are continuous at the heterojunctions as predicted by the natural interface conditions in Eqs. (8) and (9).

BenDaniel and Duke Hamiltonian. There are two finite difference representations for BenDaniel and Duke Hamiltonian: the direct difference equation (23) and the harmonic difference equation (24). The relative errors of the direct difference equation are plotted in Fig. 3 and those of the harmonic difference equation, in Fig. 4.

The results by the direct difference representation of the BenDaniel and Duke Hamiltonian exhibit similar features to the conventional Hamiltonian. The envelope functions are shown in the window of Fig. 3. The envelope functions are continuous at the abrupt junctions, but their derivatives are not. This agrees with the natural interface conditions given in Eqs. (8) and (10).

The harmonic difference equation with a proper discretization pattern shows in Fig. 4 that each eigenvalue has its own optimal N, but that none of these optimal discretization numbers coincides. Researchers working on the miscible fluids in porous media prefer the harmonic average over the direct average in dealing with the coefficient with large spatial gradient [42, 43]. We found that, for the solution to the BenDaniel and Duke Hamiltonian, the direct average provides more accurate results than the harmonic average.

Table I displays analytic and numerical solutions to the conventional Hamiltonian and the BenDaniel and Duke Hamiltonian. In the table, the numerical results only include the properly discretized FEM and FD solutions for comparison, and the finite difference solutions to the BenDaniel and Duke Hamiltonian are obtained by the direct difference equation. The table shows the results with the accuracy of about $10^{-4} = 0.01\,\%$ and the results with the best accuracy achieved in this work.

Similar FEM calculation has been done for an infinite square quantum well, using an optimal mesh pattern in Ref. [24], and it was reported that the relative error for the first eigen level is about 10^{-6} for $N = 1000$. With the same N, the relative error of the first eigenenergy of a finite square

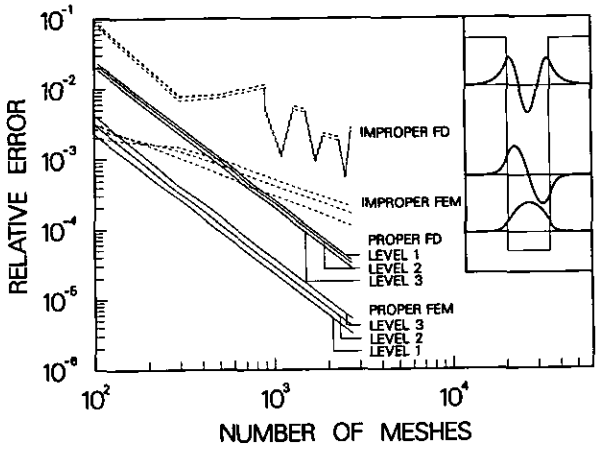

FIG. 3. *Accuracy of SQW solution using the direct difference equation of the BenDaniel and Duke Hamiltonian.* The relative error versus the discretization number using the FEM and the FD methods with proper and improper discretization patterns is depicted. The direct difference equation for the BenDaniel and Duke Hamiltonian is used for this plot. The notational conventions follow those given in Fig. 2. The envelope functions shown in the window confirm the natural boundary conditions.

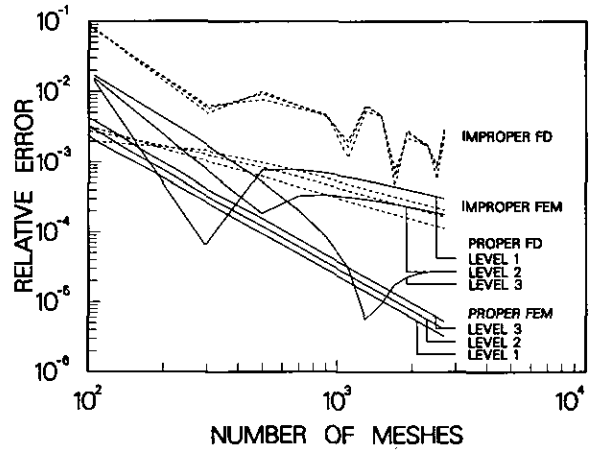

FIG. 4. *Accuracy of SQW solution using the harmonic difference equation of the BenDaniel and Duke Hamiltonian.* The relative error versus the discretization number using the FEM and the FD methods with the proper and improper discretization patterns is depicted. The harmonic difference equation for the BenDaniel and Duke Hamiltonian is used for this plot. The notational conventions follow those given in Fig. 2.

TABLE I

Solution to a SQW

		Analytic solution	FEM ($N=500$)	FD ($N=1295$)	FEM ($N=2695$)	FD ($N=2695$)
CH	E_1	0.0415523	0.0415556 (0.0080%)	0.0415471 (−0.0125%)	0.0415524 (0.0003%)	0.0415511 (−0.0029%)
	E_2	0.1603302	0.1603499 (0.0123%)	0.1603087 (−0.0134%)	0.1603309 (0.0004%)	0.1603252 (−0.0031%)
	E_3	0.3292823	0.3293301 (0.0145%)	0.3292445 (−0.0115%)	0.3292839 (0.0005%)	0.3292736 (−0.0027%)
BDDH	E_1	0.0357664	0.0357698 (0.0094%)	0.0357608 (−0.0157%)	0.0357665 (0.0003%)	0.0357651 (−0.0036%)
	E_2	0.1423513	0.1423684 (0.0120%)	0.1423313 (−0.0141%)	0.1423519 (0.0004%)	0.1423467 (−0.0033%)
	E_3	0.3110624	0.3111106 (0.0155%)	0.3110247 (−0.0121%)	0.3110641 (0.0005%)	0.3110537 (−0.0028%)

Note. The analytic solution and properly discretized FEM and FD solutions to a SQW are tabulated. N given in the first row is the number of discretizations used. CH and BDDH are the acronyms for the conventional Hamiltonian, and the BenDaniel and Duke Hamiltonian, respectively. E_i is the eigenenergy of the ith level in eV units. The percentage given in the parentheses is the relative error $(E_i - E_i^{\text{analytic}})/E_i^{\text{analytic}}$; the negative sign means that the numerical solution is smaller than the analytic solution.

quantum well is found to be about 2×10^{-5} in this paper. This deviation may be due to two reasons. First, the calculation of a finite square quantum well needs to distribute nodal points in the barriers to account for the evanescent behavior of the envelope functions. Second, the mesh pattern is not optimized.

For the calculations of SQWs with well widths and barrier heights different from this specific example, the closer the highest eigen level is to the barrier height, the larger the numerical solution domain must be used to ensure that the envelope functions decay to insignificant magnitudes at both ends.

Bastard Hamiltonian. It was shown in Eqs. (11) to (13) that the solutions to the SQW by the Bastard Hamiltonian without essentially imposed interface conditions exhibit unbounded envelope function at the heterojunctions. If this observation is ignored and the finite difference equation (25) is used to analyze a SQW, the following phenomena appear. First, the numerical scheme converges to different eigenvalues for different discretization numbers, and the eigenvalues fluctuate wildly. Second, each envelope function show two kinks at the mass discontinuities as shown in Fig. 5.

These behaviors can be explained as follows. In the finite difference method, the envelope function is assumed to be single-valued and finite at each discretization point. Therefore, the theoretically unbounded envelope functions are not tractable by using this numerical approach. This leads

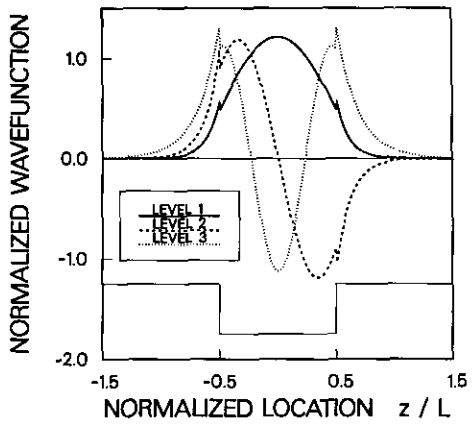

FIG. 5. *False finite difference solution of a SQW using the bastard Hamiltonian.* The bastard Hamiltonian applied to a structure with a discontinuous mass profile such as a SQW leads to unbounded envelope functions unless the interface conditions are essentially imposed. If one ignores this and applies the FD to search for the eigensolutions, each envelope function exhibits two kinks. In this plot, $N=700$ and $x_1=-x_2=3.5$.

the numerical scheme to converge to a false solution. Furthermore, in the finite difference method, a SQW is discretized as in Fig. 1; namely, the original discontinuous mass profile is approximated by a piecewise linear (C^0) profile. The solutions to the Bastard Hamiltonian for the quantum well with piecewise linear mass and potential profiles are continuous and bounded as the two differential terms in the square bracket of Eq. (5), $1/m(z)\cdot d^2\psi(z)/dz^2$ and $d^2/dz^2[\psi(z)/m(z)]$, are singular to the same order at the connection point of two linear pieces. This explains the boundedness of the false envelope functions in Fig. 5.

The appearance of the kinks in the false envelope function shown in Fig. 5 can be explained as follows. Equation (12) is generally true if the potential is a C^0 profile; namely, Eq. (12) still holds at any finite difference nodal point, z_i. Moreover, in the context of the finite difference method, the mass profile is approximated by a piecewise linear function. Hence, in the infinitesimal region encompassing a FD nodal point z_i,

$$m''(z)=\frac{dm(z)}{dz}\bigg|_{z_i^-}^{z_i^+}\cdot\delta(z-z_i)$$
$$=\left[\frac{dm(z_i^+)}{dz}-\frac{dm(z_i^-)}{dz}\right]\cdot\delta(z-z_i). \tag{28}$$

Substituting Eq. (28) to Eq. (12), it follows that

$$\left[\frac{1}{m(z)}\frac{d\psi(z)}{dz}\right]\bigg|_{z_i^-}^{z_i^+}=\frac{1}{2}\frac{\psi(z_i)}{m(z_i)^2}\cdot\left(\frac{dm(z)}{dz}\bigg|_{z_i^-}^{z_i^+}\right). \tag{29}$$

If z_i is not at the connection point of two linear segments of different slopes such as the point at z_j or z_k in Fig. 1, then $dm(z_i^+)/dz-dm(z_i^-)/dz=0$. Therefore, $m''(z)=0$ and

$d\psi(z)/dz$ is continuous. If z_i is at the connection point on the C^0 profile such as the point at $z = z_p$, z_{p-1}, z_q, or z_{q-1} in Fig. 1, then $dm(z_i^+)/dz - dm(z_i^-)/dz \neq 0$. The discontinuity of $1/m(z) \cdot d\psi(z)/dz$ is proportional to the discontinuity of $dm(z)/dz$. This explains the crinkles at the abrupt heterojunctions of the SQW.

The above arguments about the finite difference solution to the Bastard Hamiltonian hold solely due to the spatial discontinuity of the mass. The temporal dependence of the time-dependent effective mass equation does not influence the results in this aspect. We believe we have resolved the paradoxial crinkles in Fig. 1 of the paper by C. Juang *et al.* [5].

3.2. *Simple Harmonic Oscillator*

The particle mass of a SHO is independent of the particle location, thus the mass profile of a SHO is continuous in contrast to that of a SQW. The FEM [36] and the FD solutions to a SHO will be presented in this section to show that the discontinuity effects discussed in the previous subsection are indeed induced by the abrupt heterojunctions.

The quadratic potential barrier of a SHO reads,

$$V(z) = \tfrac{1}{2}kz^2, \tag{30}$$

where k is the restoring force constant. With the restoring force constant of $k = 3.0328 \times 10^{-3}$ N/m. This SHO resembles a parabolic quantum well whose potential barrier varies quadratically from 0.0 eV to 0.4 eV within a distance of 65.01 Å (23 monolayers of the *GaAs* lattice), except that the electron effective mass is assumed constant, $m = 0.067m_0$.

Since the mass is a constant, the three Hamiltonians given in Eqs. (3) to (5) reduce to an identical form, and thus have the same eigensolutions. The analytic eigenvalues of a SHO are well known, and, for the nth level, the eigenenergy is

$$E_n = \left(n + \frac{1}{2}\right)\hbar\sqrt{\frac{k}{m}}. \tag{31}$$

TABLE II

Solution to a SHO

	Analytic solution	FEM ($N = 360$)	FD ($N = 1200$)	FEM ($N = 2320$)	FD ($N = 2320$)
E_1	0.0733628	0.0733668 (0.0055%)	0.0733594 (−0.0046%)	0.0733629 (0.0001%)	0.0733619 (−0.0012%)
E_2	0.2200884	0.2201086 (0.0092%)	0.2200714 (−0.0077%)	0.2200888 (0.0001%)	0.2200839 (−0.0021%)
E_3	0.3668141	0.3668661 (0.0142%)	0.3667698 (−0.0121%)	0.3668149 (0.0002%)	0.3668022 (−0.0032%)

Note. The exact solution and FEM and FD solutions to an SHO are shown. The three Hamiltonians have the same solution. The notation used here follows the conventions of Table I.

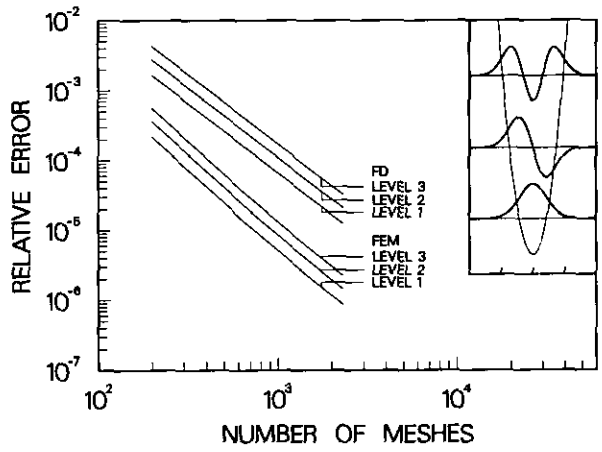

FIG. 6. *Accuracy of solution to a SHO.* The relative errors of FEM and FD solutions to a SHO are displayed as functions of the discretization numbers. Due to the assumption of a constant effective mass, the three Hamiltonians reduce to the same form. This plot can be interpreted as results for any one of the three Hamiltonians. The envelope functions are shown in the window.

The proper discretization patterns devised for the SQW are not needed for the SHO because there is no discontinuity on the mass profile. The numerical solutions show that both the finite element and the finite difference methods produce rather accurate results as given in Table II. The relative errors by the FEM and the FD are plotted in Fig. 6. Both numerical schemes show monotonous convergence as the discretization number increases. Because the numerical solutions obtained depend only on the numerical scheme and the mesh pattern, the eigenenergies tabulated in Table II and the relative errors plotted in Fig. 6 can be interpreted as results obtained by using any one of the three Hamiltonians.

By the Bastard Hamiltonian, the finite difference solutions to a SHO show that the eigenenergies converge to the analytic results and that the envelope functions as depicted in Fig. 6 possess no kink unlike the SQW solutions. Additionally, the harmonic representation of the BenDaniel and Duke Hamiltonian produces results which agree with the analytic solutions to high accuracy. As a result, the numerical solutions to a SHO confirms that the effects caused by the discontinuities of a SQW disappear in the case of a SHO.

4. CONCLUDING REMARKS

This paper has investigated the effects of the mass discontinuity on the numerical solutions to the effective mass

equation. The numerical methods investigated in this paper are the finite element method with linear basis functions and the finite difference method with the entire truncated solution domain discretized by equally spaced nodal points.

The discontinuous points of the mass profile are shown to introduce additional error if they are not properly placed in the mesh. The proper finite element discretization pattern requires that the mass dicontinuity coincide with the nodal point. Besides the above condition, the proper finite difference discretization pattern further requires that only one of the two adjacent discontinuities be considered interior to the mesh defined by them.

Two finite difference representations of the BenDaniel and Duke Hamiltonian have been explored. The direct difference equation is found more accurate than the harmonic difference equation.

It was reported that the envelope functions obtained from the finite difference equation of the Bastard Hamiltonian show crinkles at the mass discontinuities. We found that it is because the Bastard Hamiltonian has unbounded envelope function at the mass discontinuity. The finite difference equation contradictorily assumes that all nodal values are finite. Further interface conditions have to be essentially imposed at the mass discontinuity to well pose the problem using the Bastard Hamiltonian.

ACKNOWLEDGMENTS

The authors would like to express sincere appreciation to M. Luke and K. M. Shyue for discussions about the solution methods and to Dr. R. B. Darling and Dr. S. H. Lou for comments on the manuscript. This work is supported by the U.S. National Science Foundation under NSF Grant No. ECS-8909082.

REFERENCES

1. G. Bastard, *Phys. Rev. B* **24** (10), 5693 (1981).
2. R. L. Greene, K. K. Bajaj, and D. E. Phelphs, *Phys. Rev. B* **29** (4), 1807 (1984).
3. D. Mukherji and B. R. Nag, *Phys. Rev. B* **12** (10), 4338 (1975).
4. K. J. Kuhn, C. Juang, and R. B. Darling, *J. Appl. Phys.* **69** (5), 3135 (1991).
5. C. Juang, K. J. Kuhn, and R. B. Darling, *Phys. Rev. B* **41** (17), 12047 (1990).
6. G. Bastard, *Phys. Rev. B* **25** (12), 7584 (1982).
7. M. F. H. Schuurmans and G. W. 't Hooft, *Phys. Rev. B* **31** (12), 8041 (1985).
8. Z. Ikonic, V. Milanovic, and D. Tjapkin, *IEEE J. Quant. Electron.* **25** (1), 54 (1989).
9. Z. Ikonic, V. Milanovic, and D. Tjapkin, *J. Phys. C* **20**, 1147 (1987).
10. W. W. Lui and M. Fukuma, *J. Appl. Phys.* **60** (5), 1555 (1986).
11. D. Ahn and S. L. Chuang, *Phys. Rev. B* **34** (12), 9034 (1986).
12. D. Ahn and S. L. Chuang, *Phys. Rev. B* **35** (8), 4149 (1987).
13. D. A. B. Miller, D. S. Chemla, T. C. Damen, A. C. Gossard, W. Wiegmann, T. H. Wood, and C. A. Burrus, *Phys. Rev. B* **32** (2), 1043 (1985).
14. L. Quiroga, F. J. Rodriguez, A. Camacho, and C. Tejedor, *Phys. Rev. B* **42** (17), 11198 (1990).
15. T. Lukes, G. A. Ringwood, and B. Suprapto, *Physica A* **84**, 421 (1976).
16. F. M. Fernández and E. A. Castro, *Physica A* **111**, 334 (1982).
17. G. Bastard, E. E. Mendez, L. L. Chang, and L. Esaki, *Phys. Rev. B* **28** (6), 3241 (1983).
18. N. W. Ashcroft and N. D. Mermin, *Solid State Physics* (W. B. Saunders, Philadelphia, 1976), p. 332.
19. R. Kozack and F. S. Levin, *Phys. Rev. C* **36** (3), 883 (1987).
20. S. R. White, J. W. Wilkins, and M. P. Teter, *Phys. Rev. B* **39** (9), 5819 (1989).
21. F. S. Levin and J. Shertzer, *Phys. Rev. B* **32** (6), 3285 (1985).
22. W. Schulze and D. Kolb, *Chem. Phys. Lett.* **122** (3), 271 (1985).
23. A. Askar, *J. Chem. Phys.* **62** (2), 732 (1975).
24. Z. H. Levine and J. W. Wilkins, *J. Comput. Phys.* **83**, 361 (1989).
25. K. Nakamura, A. Shimizu, M. Koshiba, and K. Hayata, *IEEE J. Quant. Electron.* **25** (5), 889 (1989).
26. K. Nakamura, A. Shimizu, M. Koshiba, and K. Hayata, *IEEE J. Quant. Electron.* **27** (8), 2035 (1991).
27. T. Ando and S. Mori, *Surf. Sci.* **113**, 124 (1982).
28. O. C. Zienkiewicz and K. Morgan, *Finite Elements and Approximation*, (Wiley, New York, 1983), Chap. 6.
29. O. C. Zienkiewicz, *The Finite Element Method*, 3rd ed. (McGraw–Hill, London, 1977), Chap. 3.
30. J. Khurgin, *J. Opt. Soc. Am. B* **6** (9), 1673 (1989).
31. D. Ahn and S. L. Chuang, *J. Appl. Phys.* **64** (11), 6143 (1988).
32. Q. G. Zhu and H. Kroemer, *Phys. Rev. B* **27** (6), 3519 (1983).
33. D. J. BenDaniel and C. B. Duke, *Phys. Rev.* **152** (2), 683 (1966).
34. T. Gora and F. Williams, *Phys. Rev. B* **177** (3), 1179 (1969).
35. G. Bastard, J. K. Furdyna, and J. Mycielski, *Phys. Rev. B* **12** (10), 4356 (1975).
36. D. S. Burnett, *Finite Element Analysis from Concepts to Applications* (Addison–Wesley, Reading, MA, 1988), pp. 402, 429, 431.
37. J. J. Sakurai, *Modern Quantum Mechanics* (Benjamin/Cummings, Menlo Park, CA, 1985), pp. 17, 54, 91, 101.
38. M. Abramowitz and I. E. Stegun, *Handbook of Mathematical Functions with Formulas, Graphs, and Mathematical Tables* (National Bureau of Standards, Washington, DC, 1972), p. 916.
39. E. Merzbacher, *Quantum Mechanics*, 2nd ed. (Wiley, New York, 1970), p. 106.
40. S. Adachi, *J. Appl. Phys.* **58** (3), R1 (1985).
41. K. J. Bathe and E. L. Wilson, *Numerical Methods in Finite Element Analysis* (Prentice-Hall, Englewood Cliffs, NJ, 1976).
42. G. R. Shubin and J. B. Bell, *Comput. Methods Appl. Mech. Eng.* **47**, 47 (1984).
43. J. B. Bell, C. N. Dawson, and G. R. Shubin, *J. Comput. Phys.* **74**, 1 (1988).